NASA Technical Memorandum 88818

NASA-TM-88818 19860023126

Near-Field Spillover From a Subreflector: Theory and Experiment

S.W. Lee
University of Illinois
Urbana, Illinois

R. Acosta
Lewis Research Center
Cleveland, Ohio

A.R. Cherrette
University of Illinois
Urbana, Illinois

and

P.T. Lam
Lockheed Missiles and Space Company
Sunnyvale, California

September 1986

NASA

ENTER: X RN/NASA-TM-88818
4B▒ X €)

DISPLAY 14/6/1
86N32598*# ISSUE 24 PAGE 3714 CATEGORY 32 RPT#: NASA-TM-88818
E-3178 NAS 1.15:88818 CNT#: NAG-419 86/09/00 20 PAGES UNCLASSIFIED
DOCUMENT
UTTL: Near-field spillover from a subreflector: Theory and experiment
AUTH: A/LEE, S. W.; B/ACOSTA, R.; C/CHERRETTE, A. R.; D/LAM, P. T. PAA:
A/(Illinois Univ., Urbana); D/(Lockheed Missiles and Space Co.,
Sunnyvale, Calif.)
CORP: National Aeronautics and Space Administration. Lewis Research Center,
Cleveland, Ohio.
SAP: Avail: NTIS HC A02/MF A01
CIO: UNITED STATES
MAJS: /*ANTENNA RADIATION PATTERNS/*NEAR FIELDS/*NUMERICAL ANALYSIS
MINS: / INCIDENT RADIATION/ REFLECTOR ANTENNAS/ SUBREFLECTORS
ABA: Author

NEAR-FIELD SPILLOVER FROM A SUBREFLECTOR: THEORY AND EXPERIMENT*

S.W. Lee
University of Illinois
Department of Electrical and Computer Engineering
Urbana, Illinois 61801

R. Acosta
National Aeronautics and Space Administration
Lewis Research Center
Cleveland, Ohio 44135

A.R. Cherrette
University of Illinois
Department of Electrical and Computer Engineering
Urbana, Illinois 61801

and

P.T. Lam
Lockheed Missiles and Space Company
Sunnyvale, California

SUMMARY

In a dual reflector antenna, the spillover from the subreflector is important in determining the accuracy of near-field measurements. This is especially so when some of the feed elements are placed far away from the focus. In this paper, we present a high-frequency GTD analysis of the spillover field over a plane just behind the subreflector. Special attention is given to the field near the incident shadow boundary and the role played by the slope diffraction term. Our computations are in excellent agreement with experimental results.

E-3178

INTRODUCTION

Some dual-reflector antennas for space or radar applications have very large diameters in terms of wavelength (100λ or more). They are usually tested in a near-field range. The far-field radiation patterns are extracted mathematically from the near-field measurement data. A typical near-field setup is shown in figure 1. The total field at a typical point C (fig. 2) at the near-field recording plane consists of two contributions: the direct field from the main reflector (such as the field on ray ADEC), and the spillover from the subreflector. At high frequencies, the latter can be further separated into two components: the direct field from the feed on ray AC, and the edge diffracted from the rim of the subreflector on ray ABC. In many cases, the spillover is small, and, therefore, is traditionally neglected in near-field studies. However, there is an ever-increasing number of situations where the spillover must be taken into consideration. Two examples are:

---

*This work was supported by NASA Grant NAG-419.

(1) For an ultra-low sidelobe antenna, the wide-angle sidelobes are actually determined by the small spillover.

(2) To achieve a wide angle scan, many feed elements are placed away from the focus, and, consequently, the spillover is no longer small.

It is the purpose of this paper to study this spillover both theoretically and experimentally.

Referring to figure 3, we shall derive a complete GTD analysis for the total diffracted field at a point C on the near-field recording plane. The feed location A is arbitrary and the subreflector surface is also arbitrary. This analysis is very similar to one described in reference 1. The difference is that, in the present analysis, the observation point C may fall on the incident shadow boundary (in contrast to the reflected shadow boundary in the analysis of ref. 1); therefore, uniform theories (refs. 2 to 4) must be used there.

An analysis is given for a simple configuration (hyperbolic reflector with a point feed at a focus) and nominal results presented. However, more general configurations are also included.

SPECIAL CASE: HYPERBOLIC SUBREFLECTOR

The near-field calculation from a subreflector by GTD is very lengthy and tedious, because of the three dimensional configuration and the arbitrariness in the feed and observation locations. We have developed a computer code for doing such a calculation. In the present section, let us concentrate on a special configuration, whose solution is simple enough to bring out the physical significance of various parameters.

The configuration is shown in figure 4. A symmetrical hyperbolic subreflector is described by

$$z = f + b\sqrt{1 + \frac{x^2 + y^2}{f^2 - b^2}}, \quad \text{for } x^2 + y^2 \le a^2 \tag{2.1}$$

Here $2f$ is the distance between foci, $2b$ is that between vertices, and a is the radius of the circular aperture. The eccentricity of the hyperboloid is defined by f/b. The exterior wedge angle of the reflector is $m\pi$. For the special case in which $m = 2$, the wedge becomes a thin edge. The point feed is at a focus A. The incident field from it at an observation point $(r, \theta, \phi = 0)$ is given by (for $\exp j\omega t$ time convention)

$$\vec{E}^i(r, \theta, \phi = 0) = \frac{e^{-jkr}}{kr}\left[\hat{\theta}P_\theta(\theta) + \hat{\phi}P_\phi(\theta)\right] \tag{2.2}$$

Here $P_\theta(\theta)$ is the E-plane pattern and P_ϕ is the H-plane pattern of the feed. The problem at hand is to calculate the total field $\vec{E}^t$ at a near-field point C, whose conditions are $(x = x, y = 0, z = c)$.

The parameters a, b, c, f, x, and m describe the geometry completely. For them, the following secondary geometrical parameters can be deduced (figs. 4 and 5):

Distances:

$$\ell_1 = [a^2 + (\ell_4 + 2f)^2]^{1/2}$$

$$\ell_2 = [(x - a)^2 + (c - \ell_4)^2]^{1/2}$$

$$\ell_3 = [x^2 + (c + 2f)^2]^{1/2}$$

$$\ell_4 = -f + b\sqrt{1 + \frac{a^2}{f^2 - b^2}}$$

$$\ell_5 = \frac{a(2f + c)}{(2f + \ell_4)}$$

$$\ell_6 = \frac{\ell_1(c - \ell_4)}{(2f + \ell_4)} \qquad (2.3)$$

Diffraction angles:

$$\Psi^i = [\mathrm{sgn}(\ell_5 - x)] \cos^{-1}\left[\frac{a(x - a) + (sf + \ell_4)(c - \ell_4)}{\ell_1 \ell_2}\right]$$

$$\Psi^r = \pi - 2\theta_4 + \Psi^i$$

$$\theta_4 = \cos^{-1}\frac{2f + \ell_4 - ag'}{\ell_1\sqrt{1 + g'^2}}$$

$$g' = \frac{ab}{\sqrt{(f^2 - b^2)(f^2 - b^2 + a^2)}} \qquad (2.4)$$

Note that Ψ^i, defined in equation (2.4), obeys the following sign convention: Ψ^i is positive if observation point C is in the shadow region of $\vec{E}^i$, and is negative if C is in the lit region. For the present application, C is always in the shadow region of the reflected field $\vec{E}^r$ and, hence, Ψ^r defined in equation (2.4) is positive.

Let us now calculate the Keller's edge diffracted field $\vec{E}^d$ at C. There are two diffraction points: B and a corresponding point at the lower edge. In the present application, the lower edge is very weakly illuminated, and its contribution is therefore ignored. For the diffracted pencil emanated from b, the interfocal distance R calculated from equation (4.7) of reference 3 is

$$\frac{1}{R} = \frac{1}{\ell_1} + \frac{\left[\frac{(ag' - 2f - \ell_4)}{\ell_1}\right] + \left[\frac{(c - \ell_4 + g'a - g'x)}{\ell_2}\right]}{a\sqrt{1 + g'^2}} \qquad (2.5)$$

The diffraction coefficients as calculated from equation (4.10) of reference 3 are:

$$x^{i,r} = \frac{\frac{2}{m}\sin\frac{\pi}{m}}{\cos\frac{\pi}{m} - \cos\frac{\pi + \psi^{i,r}}{m}} \tag{2.6}$$

The diffracted field at C is calculated from equation (4.8) of reference 3.

The final result is

$$\vec{E}^d(C) = \frac{e^{-j(k\ell_2 + \pi/4)}}{2\sqrt{2\pi k\ell_2}} \frac{1}{\sqrt{1 + (\ell_2/R)}}$$

$$\cdot \left[\left(\hat{x}\frac{C - \ell_4}{\ell_2} - \hat{z}\frac{n - a}{\ell_2}\right)(x^i + x^r)\, E^i_\theta(B) + \hat{y}\,(x^i - x^r)\, E^i_\phi(B)\right] \tag{2.7}$$

where

$$\begin{bmatrix} E^i_\theta(B) \\ \\ E^i_\phi(B) \end{bmatrix} = \frac{e^{-jk\ell_1}}{k\ell_1} \begin{bmatrix} P_\theta(\theta_1) \\ \\ P_\phi(\theta_1) \end{bmatrix}$$

$$\theta_1 = \sin^{-1}\left(\frac{a}{\ell_1}\right)$$

According to UAT reference 3, the total field $\vec{E}^t$ at C is the sum of the Keller's diffracted field $\vec{E}^d$ in equation (2.7) and a modified geometrical optics field $\vec{E}^G$ such that

$$\text{UAT:}\quad \vec{E}^t(C) = \vec{E}^G(C) + E^d \tag{2.8}$$

Here $\vec{E}^G$ is given by

$$\vec{E}^G(C) = [F(\zeta) - \hat{F}(\zeta)]\, \vec{E}^i(C) \tag{2.9}$$

The detour parameter is defined by

$$\zeta = \text{sgn}(\ell_5 - x)\Big/\sqrt{k(\ell_1 + \ell_2 - \ell_3)\,|} \tag{2.10}$$

The Fresnel function is defined by

$$F(x) = \frac{e^{j\pi/4}}{\pi} \int_x^\infty e^{-jt^2} dt \tag{2.11}$$

Its leading asymptotic expansion for $x \to \infty$ is

$$\hat{F}(x) = \frac{1}{2x\sqrt{\pi}} \exp\left[-j\left(x^2 + \frac{\pi}{4}\right)\right] \tag{2.12}$$

A polynominal approximation of $F(x)$ is, for $X > 0$,

$$F(-x) = 1 - F(x) \tag{2.13a}$$

$$F(x) \approx \frac{1}{2} e^{-jx^2} [(f_1 + f_2) - j(f_1 - f_2)] \tag{2.13b}$$

where

$$f_1(x) = \frac{(1 + 0.739x)}{(2 + 1.430x + 1976x^2)}$$

$$f_2(x) = \frac{1}{(2 + 3.305x + 2.223x^2 + 3.388x^3)}$$

In summary, for the diffraction problem in figure 4, the total field at C is given by equation (2.8). This solution is derived based on UAT, and is valid for observation points on line CD, including the transition region around the incident boundary D.

FIELD ON INCIDENT SHADOW BOUNDARY

For the hyperbolic reflector in figure 4, let us calculate the total field at D, the point exactly on the incident shadow boundary. In the absence of the reflector, the incident field from the source at point A is given by (fig. 6)

$$\vec{E}^i(D) = \frac{e^{-jk(\ell_1 + \ell_6)}}{k(\ell_1 + \ell_6)} [\hat{\theta}P_\theta(\theta_1) + \hat{\phi}P_\theta(\theta_1)] = \hat{\theta}E^i_\theta(D) + \hat{\phi}E^i_\theta(D) \tag{3.1}$$

When the reflector is present, the total field $\vec{E}^t(D)$ can be calculated from equation (2.8). Both $\vec{E}^G$ and $\vec{E}^d$ become singular at D, but their singularities cancel each other. The total field is finite and continuous there. Omitting the derivations, we give the final results below. For the θ-component (component perpendicular to the edge), the normalized total field at D is

$$\text{VAT:} \quad \frac{E^t_\theta(D)}{E^i_\theta(D)} = A_0 + \frac{e^{-j\pi/4}}{2\sqrt{2\pi k\ell_6\left(1 + \frac{\ell_6}{\ell_1}\right)}} [A_1 + A_2 + A_3] \tag{3.2}$$

where

$$A_0 = \frac{1}{2}$$

$$A_1 = 2\left(\frac{\ell_6}{\ell_1}\right)\frac{P'_\theta(\theta_1)}{P_\theta(\theta_1)}$$

$$A_2 = \left(\frac{\ell_6}{\ell_1}\right)\cot\theta_1 - \left[1 + \left(\frac{\ell_6}{\ell_1}\right)\right]\frac{1}{m}\cot\frac{\pi}{m}$$

$$A_3 = \chi^r\left[1 + \left(\frac{\ell_6}{\ell_1}\right)\right]$$

$$P'_\theta(\theta) = \frac{d\,P_\theta(\theta)}{d\theta}$$

The diffraction coefficient χ^r is defined in equation (2.6) and diffraction angle ψ^r in equation (2.4). For the ϕ-component (component parallel to the edge), the same expression equation (3.2) holds except for the following replacements:

$$E_\theta^{i,t} \to E_\phi^{i,t},\ P_\theta \to P_\theta,\ \chi^r \to (-1)\chi^r \tag{3.3}$$

Several remarks about the solution in equation (3.2) are in order.

(1) Solution (3.2) is a high-frequency asymptotic solution, accurate only to the order of $k^{-1/2}$.

(2) The solution is not valid if observation point D approaches edge point B. It does not satisfy the proper edge condition at B.

(3) The dominant term A_0 in equation (3.2) gives one half of the incident field, a well-known fact. The remaining terms are of order $k^{-1/2}$. Their contribution decreases as the source point A moves away from the edge ($\ell_1 \to \infty$).

(4) The term A_1 is proportional to the angular slope of the pattern function $P_\theta(\theta)$ of the incident field. It is sometimes known as the slope diffraction contribution.

(5) If UTD reference 4 is applied to the problem in figure 4, the corresponding solution again has the form of equation (3.2) except that terms A_1 and A_2 are absent.[1]

---

[1]The slope diffraction coefficient d_s (or d_h) in equation (7) of reference 5 cannot be used to calculate the field on the incident shadow boundary, because d_s is undefined there. This is due to the fact that D_s of UTD has a step discontinuous across the incident shadow boundary in order to cancel the step discontinuity of the geometrical optics field. The angular derivative of D_s does not exist there.

Let us present some numerical results calculated from equation (3.2). The subreflector parameters are (fig. 4)

$$a = 12\lambda, \; b = 5\lambda, \; f = 12\lambda$$

Some deduced parameters are (fig. 4 is to scale)

$$\ell_1 = 22.8\lambda, \; m\pi = 360° - 18.7° = 1.8961\,\pi \tag{3.4}$$

$$\theta_1 = 31.7°, \; \psi^r = 79.14°$$

The pattern of the incident field is assumed to be

$$P_\theta(\theta) \text{ or } P_\phi(\theta) = [\cos(\theta - \theta_0)]^{20} \tag{3.5}$$

where $\theta = \theta_0$ is the main beam direction. The 3 dB beamwidth of the incident beam is 21.3°. Thus, instead of a local plane wave, the magnitude of the incident field has a rapid angular variation.

Figure 7 shows the importance of the slope diffraction term A_1 in equation (3.2). For the present case, A_1 reads

$$A_1 = 2\left(\frac{\ell_6}{\ell_2}\right)(20)\tan(\theta_0 - \theta_1) \tag{3.6}$$

When $\theta_0 = \theta_1 = 31.7°$, term A_1 is zero and we find

$$\frac{E_\theta^t(D)}{E_\theta^i(D)} = 0.573e^{-j6.9°} \tag{3.7a}$$

$$\frac{E_\phi^t(D)}{E_\phi^i(D)} = 0.458e^{+j5.6°} \tag{3.7b}$$

Had the slope diffraction been ignored, the total field would have been given by equation (3.7) for all values of beam direction θ_0. Figure 7 shows that the normalized field increases indefinitely as the beam sweeps from the shadow side to the lit side. When $\theta_0 = 90° + \theta_1$, the incident field $E_\theta^i(D)$ or $E_\phi^i(D)$ is zero in accordance with equation (3.5), but the total field at D is not zero. Hence, the normalized field is infinite.

In figure 8, the incident beam is displaced by one beamwidth (21.3°) on either side of the shadow boundary. Note that the field is stronger when the beam is displaced to the lit side. When the observation point D moves far away from the edge, solution (3.2) approaches its far-field value, namely,

$$\frac{E_\theta^t(D)}{E_\theta^i(D)} = \frac{1}{2} + \frac{e^{-j\pi/4}}{2\sqrt{2\pi k\ell_1}}\left(2\frac{P_\theta^1}{\ell_\theta} + \cot\theta_1 - \frac{1}{m}\cot\frac{\pi}{m} + \chi^r\right), \left(\frac{\ell_6}{\ell_1}\right) \to \infty \tag{3.8}$$

This asymptotic behavior can be seen from figure 8.

NUMERICAL RESULTS AND EXPERIMENTS

Parameters of the experimental hyperbolic reflector (fig. 9) are sketched in figure 10.

$$a = 50.54", \qquad b = 23.39", \qquad f = 24.32" \tag{4.1}$$

$$\text{Eccentricity} = \frac{f}{b} = 1.04$$

There are two feeds: one for 20 GHz ($\lambda = 0.59"$) and the other for 30 GHz ($\lambda = 0.39"$). Their E-plane patterns $P_\theta(\theta)$ and the H-plane patterns $P_\phi(\theta)$ are described by

$$[\cos(\theta - \theta_0)]^q \tag{4.2}$$

where $\theta_0 = 43.5°$. Thus, the beam is 8° displaced from the incident shadow boundary. The values of q and beamwidths are shown in the following table.

	q		3 dB beamwidth	
	E-plane	H-plane	E-plane	H-plane
20 GHz	125	69	8.5°	11.5°
30 GHz	136	125	8.2°	8.5°

The fields behind the subreflector over a planar surface were measured at the NASA Lewis near-field facility. Corresponding theoretical values are calculated from equations (2.8), (2.9), and (2.7). Results are presented in figures 11 to 13. The agreement between theory and experiment is excellent.

The computer program used to calculate the theoretical values is quite general. As an example consider the modified subreflector-feed geometry shown in figure 14. Here the feed has been moved up 12 in. in the y-direction and repointed along the incident shadow boundary. The feed pattern half-power beam width has also been increased to 42.2°. Figure 15 depicts the amplitude of E_x for this set of conditions at 30 GHz.

CONCLUSION

(1) Based on UAT, we have developed a near-field spillover analysis for an arbitrarily shaped subreflector with a feed at an arbitrary location (fig. 2). A typical result is shown in figure 14.

(2) For the special case in which the subreflector is hyperbolic and the feed is on focus, explicit solutions were given. The total field at the observation point C in figure 3 is given in equation (2.8), (2.9), and (2.7).

(3) Special attention is given to the field at point D (fig. 5) on the incident shadow boundary. As described in equation (3.2), the slope diffraction term A_1 plays an important role when the incident beam has a rapidly varying pattern.

(4) An excellent agreement is obtained between the theoretical and the measured results (figs. 11 to 13) for fields just behind a large hyperbolic subreflector, which is illuminated by a field with a rapid angular variation.

REFERENCES

1. Lee, S.W., et al.: Diffraction by an Arbitrary Subreflector: GTD Solution. IEEE Trans. Antennas Propag., vol. AP-27, no. 3, May 1979, pp. 305-316. (See also correction in vol. AP-34, p. 272, 1986.)

2. Ahluwalia, D.S.; Lewis, R.M.; and Boersma, J.: Uniform Asymptotic the Theory of Diffraction by a Plane Screen. SIAM J. Appl. Math., vol. 16, no. 4, July 1968, pp. 783-807.

3. Lee, S.W.; and Deschamps, G.A.: A Uniform Asymptotic Theory of Electromagnetic Diffraction by a Curved Wedge. IEEE Trans. Antennas Propag., vol. AP-24, no. 1, Jan. 1976, pp. 25-34.

4. Kouyoumjian, R.G.; and Pathak, P.H.: A Uniform Geometrical Theory of Diffraction for an Edge in a Perfectly Conducting Surface. Proc. IEEE, vol. 62, no. 11, Nov. 1974, pp. 1448-1461.

5. Cashman, J.D.: Comments on "A Uniform Geometrical Theory of Diffraction for an Edge in a Perfectly Conducting Surface." IEEE Trans. Antennas Propag., vol. AP-25, no. 5, May 1977, pp. 447-451.

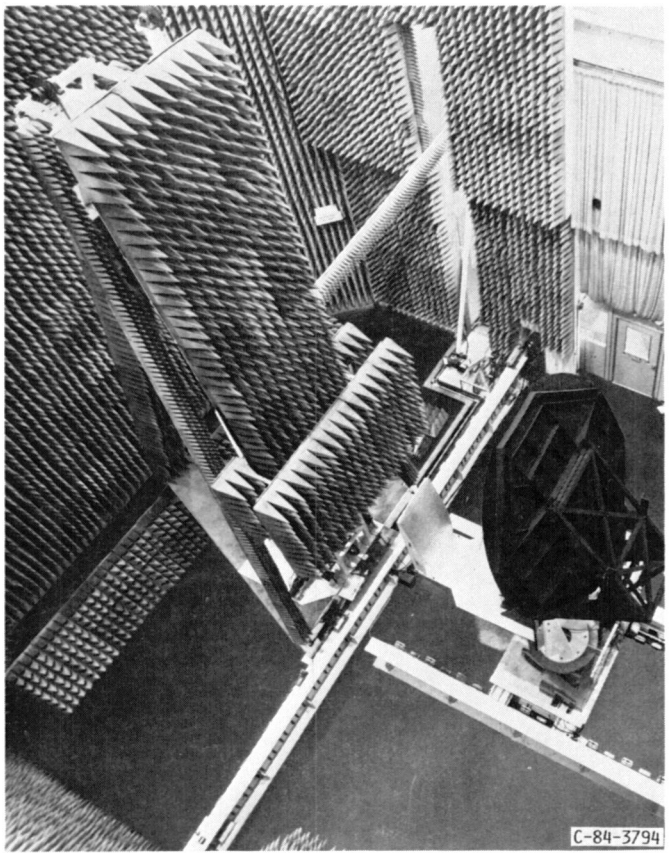

FIGURE 1. - NASA LEWIS RESEACH CENTER NEAR-FIELD MEASUREMENT FACILITY.

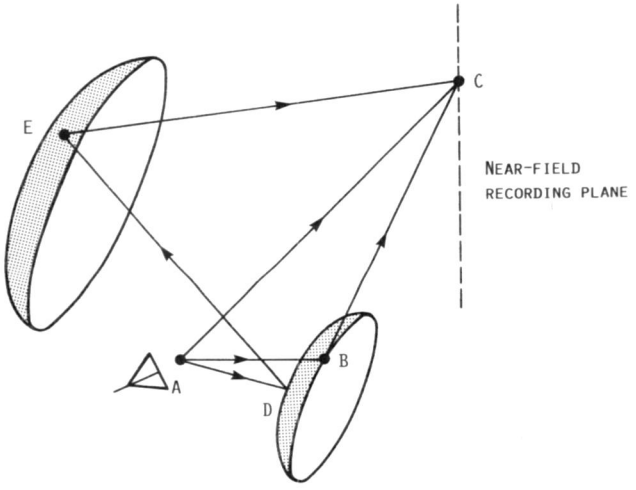

FIGURE 2.- NEAR-FIELD MEASUREMENT OF RADIATION FROM A DUAL-REFLECTOR ANTENNA.

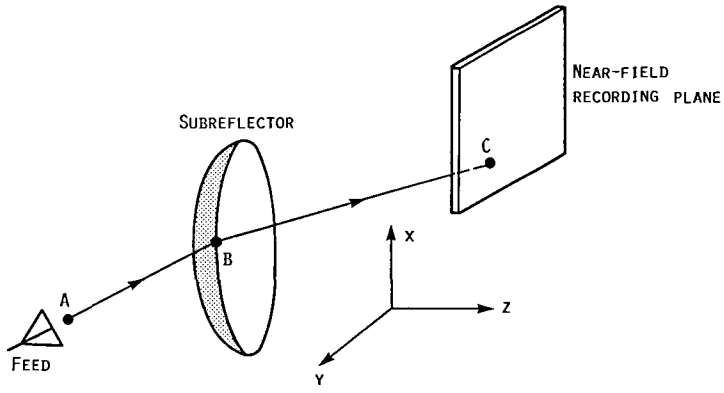

FIGURE 3.- NEAR-FIELD DIFFRACTION BY AN ARBITRARY SUBREFLECTOR.

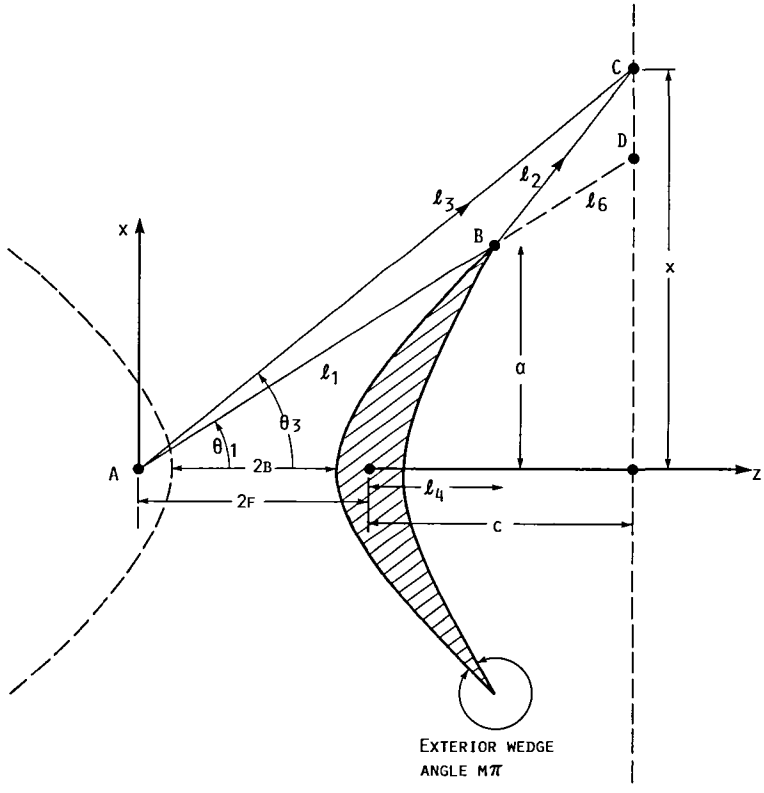

FIGURE 4.- A HYPERBOLIC SUBREFLECTOR WITH ROTATING SYMMETRY ABOUT Z-AXIS. THE RADIUS OF THE CIRUCLAR APERTURE IS A.

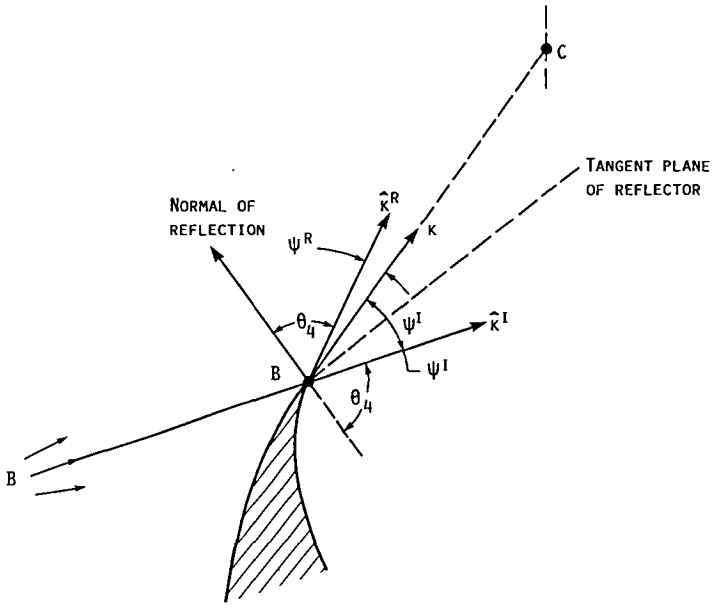

FIGURE 5.- DIFFRACTION ANGLES ψ^I AND ψ^R. DARK HALF OF ARROW $\hat{K}^I$ (OR $\hat{K}^R$) INDICATES SHADOW SIDE OF $\vec{E}^I$ (OR $\vec{E}^R$).

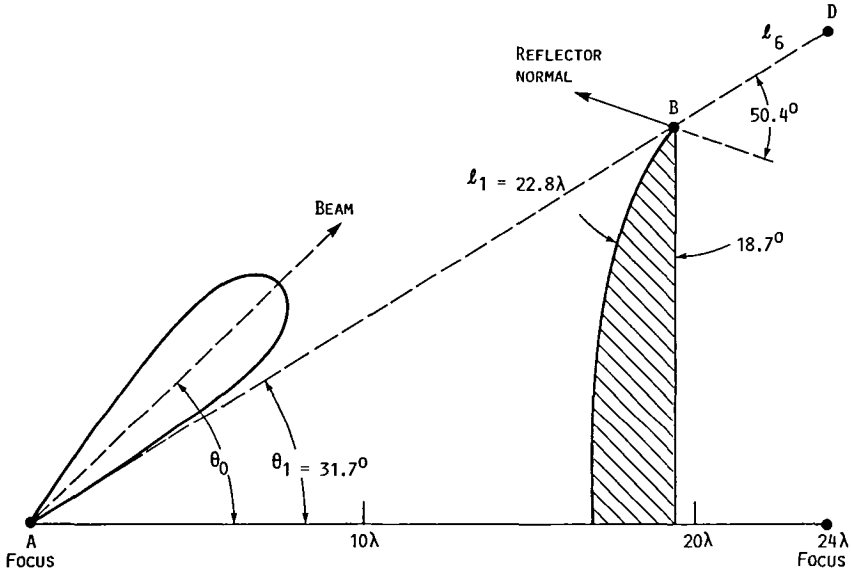

FIGURE 6.- FIELD AT D ON THE INCIDENT SHADOW BOUNDARY FOR A HYPERBOLIC SUBREFLECTOR ILLUMINATED BY A SOURCE AT FOCUS A.

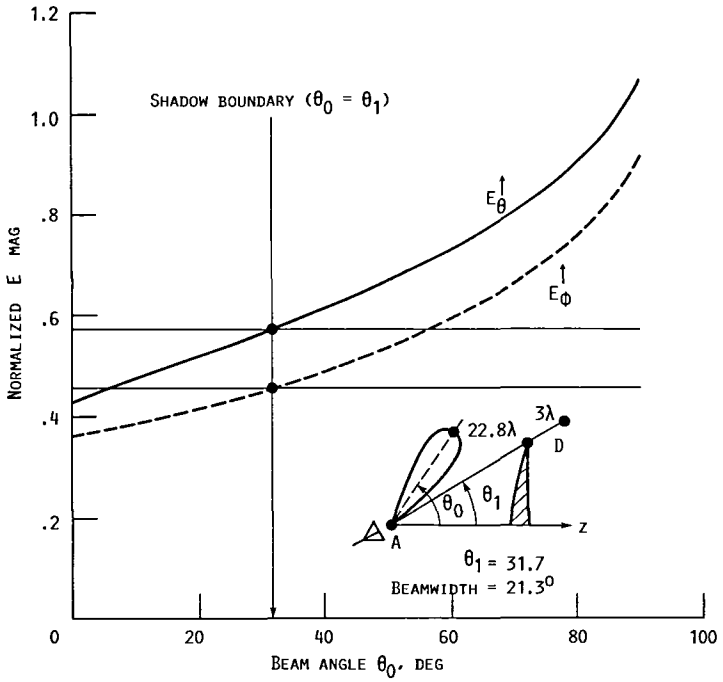

FIGURE 7.- TOTAL FIELD AT POINT D ON THE INCIDENT SHADOW BOUNDARY, NORMALIZED WITH RESPECT TO THE INCIDENT FIELD AT D FOR THE CONFIGURATION IN FIGURE 5.

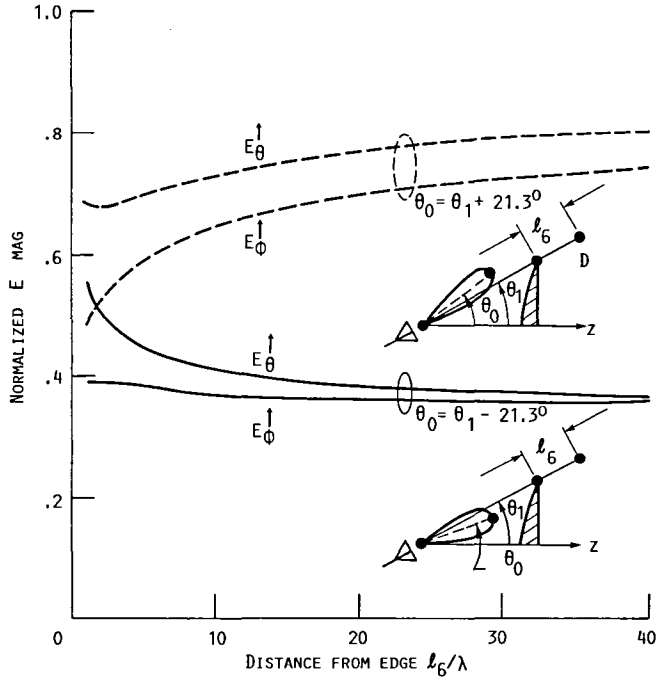

FIGURE 8.- TOTAL FIELD AT POINT D ON THE INCIDENT SHADOW BOUNDARY, NORMALIZED WITH RESPECT TO THE INCIDENT FIELD AT D FOR CONFIGURATION IN FIGURE 5. INCIDENT BEAM DIRECTION IS DISPLACED BY ONE BEAMWIDTH (21.3°) ON EITHER SIDE OF THE SHADOW BOUNDARY.

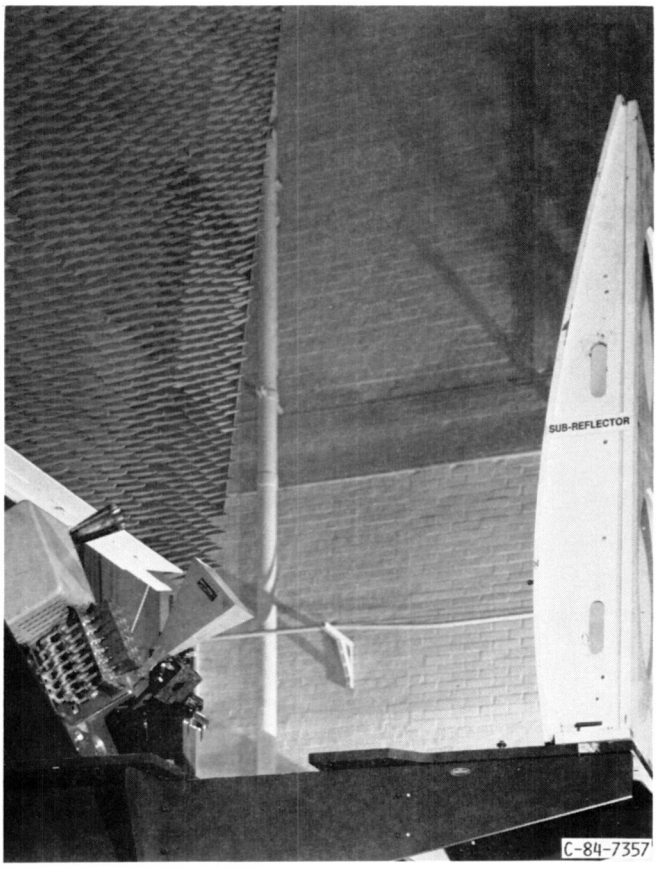

FIGURE 9. - EXPERIMENTAL HYPERBOLIC REFLECTOR AT THE NASA LEWIS RESEARCH CENTER NEAR-FIELD FACILITY.

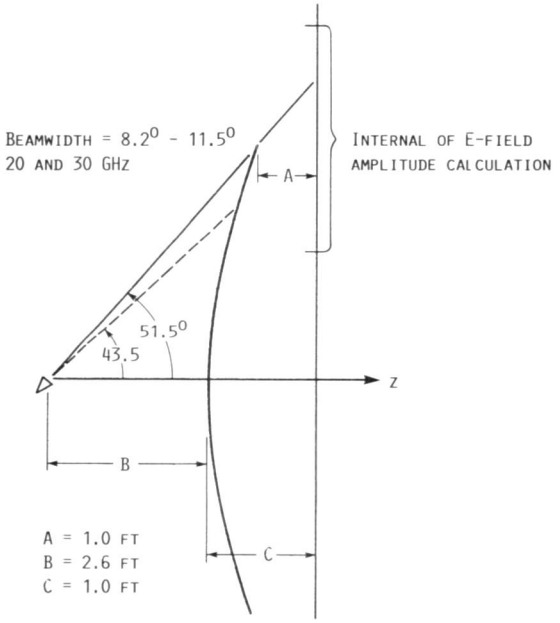

FIGURE 10.- HYPERBOLIC SUBREFLECTOR USED IN A NASA-LEWIS EXPERIMENT.

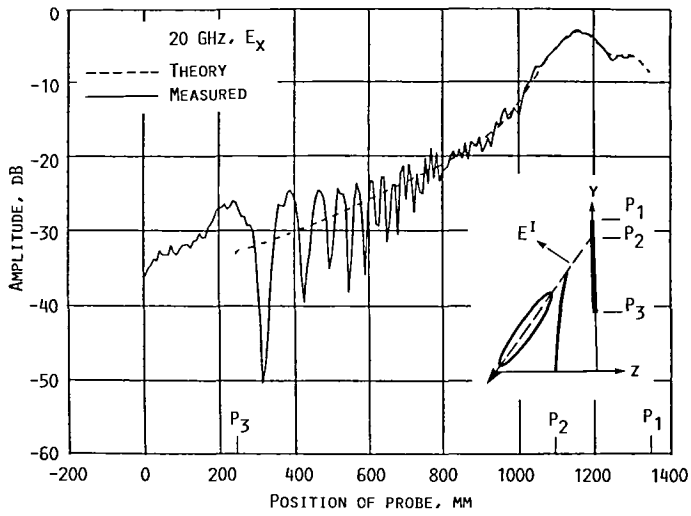

FIGURE 11A.- NEAR-FIELD E-PLANE DIFFRACTION PATTERN (E_x AT 20 GHz FOR THE CONFIGURATION IN FIGURE 8.

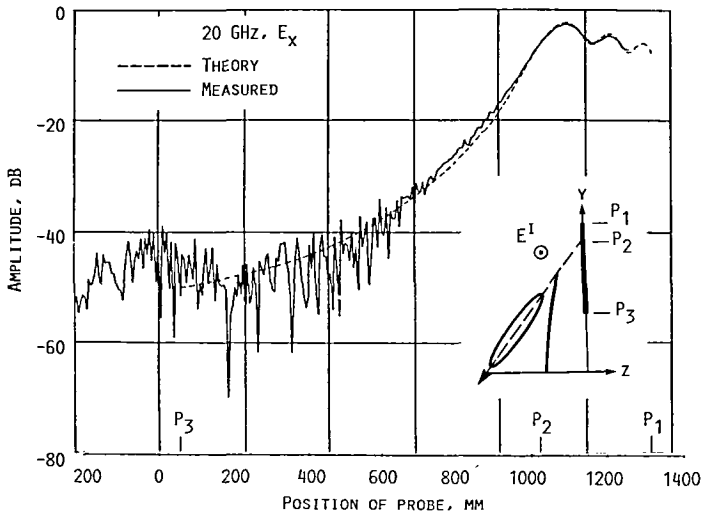

FIGURE 11B.- SAME AS FIGURE 9A EXCEPT FOR H-PLANE DIFFRACTION PATTERN (E_y COMPONENT).

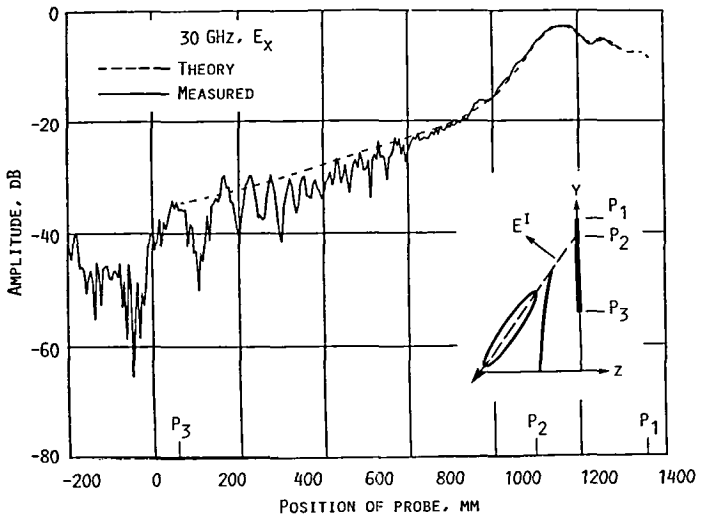

FIGURE 12A.- NEAR-FIELD E-PLANE DIFFRACTION PATTERN (E_x COMPONENT) AT 30 GHZ FOR THE CONFIGURATION IN FIGURE 8.

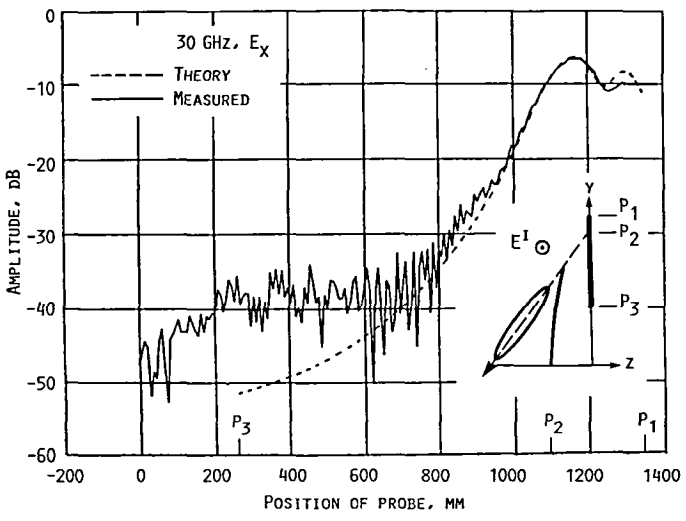

FIGURE 12B.- SAME AS FIGURE 10A EXCEPT FOR H-PLANE DIFFRACTION PATTERN (E_y COMPONENT).

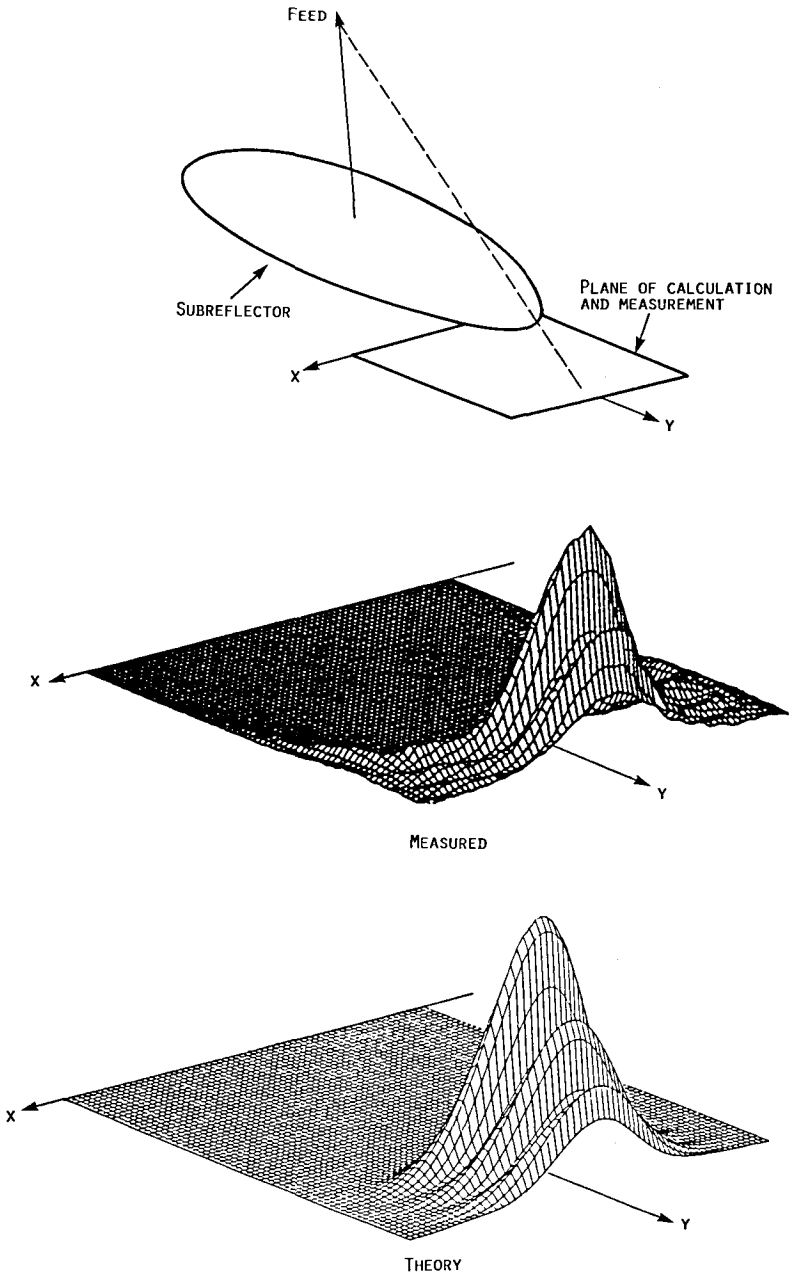

FIGURE 13.- NEAR-FIELD DIFFRACTION PATTERN OF THE SUBREFLECTOR IN FIGURE 8 WHEN IT IS ILLUMINATED BY A FEED POLARIZED IN THE Y-DIRECTION AT 30 GHz.

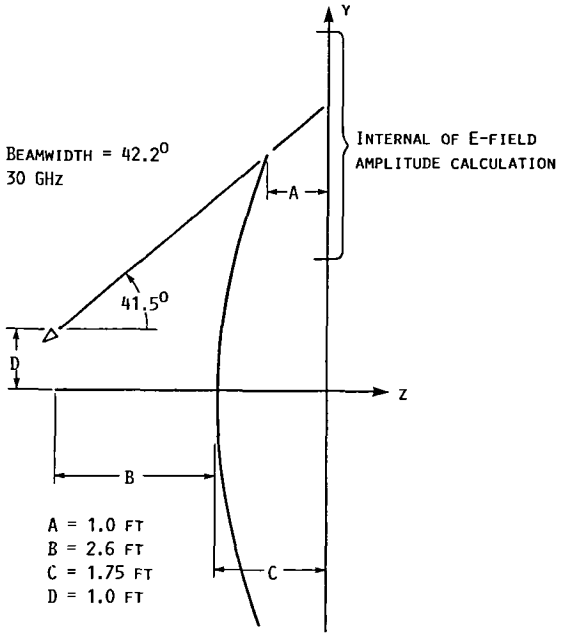

FIGURE 14.- MODIFIED HYPERBOLIC SUBREFLECTOR GEOMETRY.

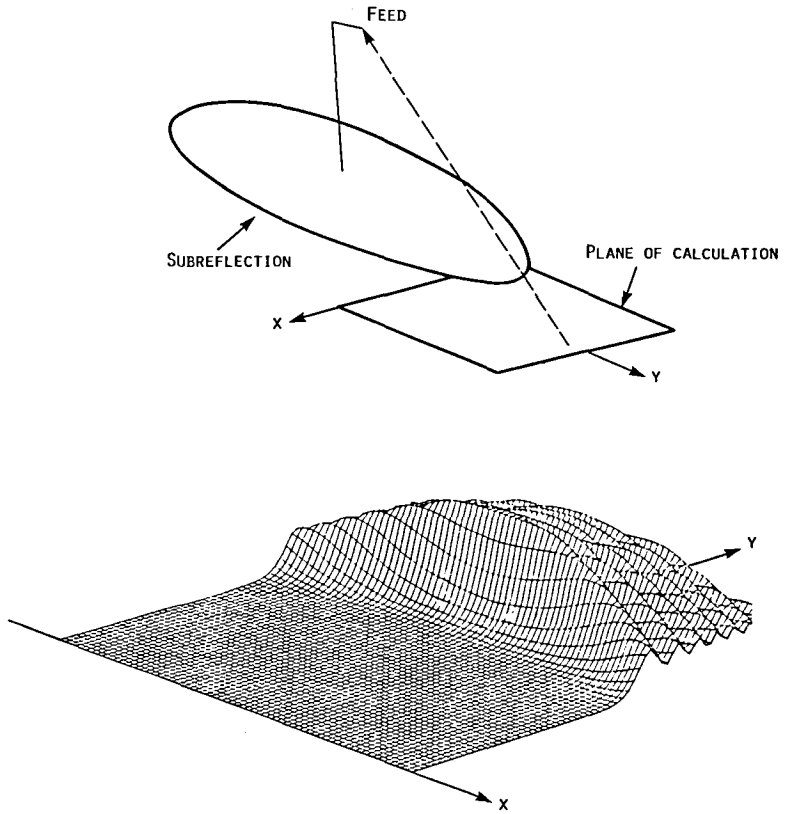

FIGURE 15.- CALCULATED NEAR-FIELD DIFFRACTION PATTERN OF THE SUBREFLECTOR IN FIGURE 12 WHEN IT IS ILLUMINATED BY A FEED POLARIZED IN THE X-DIRECTION.

1. Report No.	2. Government Accession No.	3. Recipient's Catalog No.
NASA TM-88818		

4. Title and Subtitle	5. Report Date
Near-Field Spillover From a Subreflector: Theory and Experiment	September 1986
	6. Performing Organization Code: 506-58-22

7. Author(s)	8. Performing Organization Report No.
S.W. Lee, R. Acosta, A.R. Cherrette, and P.T. Lam	E-3178
	10. Work Unit No.

9. Performing Organization Name and Address	11. Contract or Grant No.
National Aeronautics and Space Administration Lewis Research Center Cleveland, Ohio 44135	
	13. Type of Report and Period Covered: Technical Memorandum
12. Sponsoring Agency Name and Address	14. Sponsoring Agency Code
National Aeronautics and Space Administration Washington, D.C. 20546	

15. Supplementary Notes

S.W. Lee and A.R. Cherrette, University of Illinois, Dept. of Electrical and Computer Engineering, 1406 West Green St., Urbana, Illinois 61801; R. Acosta, NASA Lewis Research Center; P.T. Lam, Lockheed Missiles and Space Company, Sunnyvale, California. This work was supported by NASA Grant NAG-419.

16. Abstract

In a dual reflector antenna, the spillover from the subreflector is important in determining the accuracy of near-field measurements. This is especially so when some of the feed elements are placed far away from the focus. In this paper, we present a high-frequency GTD analysis of the spillover field over a plane just behind the subreflector. Special attention is given to the field near the incident shadow boundary and the role played by the slope diffraction term. Our computations are in excellent agreement with experimental results.

17. Key Words (Suggested by Author(s))	18. Distribution Statement
Antenna radiation patterns Near-field analysis Numerical analysis	Unclassified - unlimited STAR Category 32

19. Security Classif. (of this report)	20. Security Classif. (of this page)	21. No. of pages	22. Price*
Unclassified	Unclassified		

*For sale by the National Technical Information Service, Springfield, Virginia 22161

National Aeronautics and
Space Administration

Lewis Research Center
Cleveland, Ohio 44135

SECOND CLASS MAIL

ADDRESS CORRECTION REQUESTED

Official Business
Penalty for Private Use $300

Postage and Fees Paid
National Aeronautics and
Space Administration
NASA-451

NASA